Bremsstrahlung-induced fission and spallation of the pre-actinide nucleus ^{181}Ta

A. Deppman,[*] G. S. Karapetyan,[†] V. Guimarães,[‡] and C. Gonzales[§]
Instituto de Fisica, Universidade de São Paulo, Post Office Box 66318, 05315-970 São Paulo, Brazil

A. R. Balabekyan[‖]
Yerevan State University, Faculty of Physics, Alex Manoogian 1, Yerevan 0025, Armenia

N. A. Demekhina[¶]
Yerevan Physics Institute, Alikhanyan Brothers 2, Yerevan 0036, Armenia and
Joint Institute for Nuclear Research (JINR), Flerov Laboratory of Nuclear Reactions (LNR), Joliot-Curie 6, Dubna 141980, Moscow Region, Russia

(Received 28 November 2014; revised manuscript received 26 January 2015; published 27 February 2015)

A study of photofission on ^{181}Ta induced by bremsstrahlung with endpoint energies of 50 and 3500 MeV has been performed. The fission yields have been measured by using the induced-activity method in an off-line analysis. The total photofission yields for the tantalum target at 50 and 3500 MeV are found to be 5.4 ± 1.1 μb/equivalent quanta per second (eq.q) and 0.77 ± 0.11 mb/eq.q, respectively, and the corresponding deduced fissilities are $(0.23 \pm 0.05) \times 10^{-3}$ and $(2.9 \pm 0.5) \times 10^{-3}$. Mass- and charge-yield distributions were derived from the data. The results were compared with the simulated results from the CRISP code for multimodal fission by the assuming symmetrical fission mode.

DOI: 10.1103/PhysRevC.91.024620 PACS number(s): 25.85.Jg, 24.75.+i, 25.40.Sc, 27.70.+q

I. INTRODUCTION

Induced fission has been studied over the years for a wide variety of projectiles and energy ranges. The information obtained from these experiments encompassed different characteristics of the fissioning system. Photofission is one of the most powerful tools for studying the fission process because of the well-known spin selectivity of the excitation and the absence of the Coulomb barrier. Photons interact with nuclei by the quasideuteron mechanism and meson production. The main experimental problem in photofission studies is the lack of an intense source of monochromatic photons. Therefore, a large amount of photofission mass-yield distributions have been measured with bremsstrahlung spectra with a continuous energy distribution in the energy range of 300 to 1800 MeV [1–4]. Related to photofission on heavy nuclei, many works have been performed with monochromatic photons at intermediate and high-energy regime, using different experimental techniques [5–9]. In these experiments, the photofission yields and related fissility (the ratio of fission yields to total nuclear photoabsoption yields), were determined for pre-actinide targets with fissility parameter $Z^2/A < 31.6$. At low photon incident energies ($\leqslant$30 MeV), pre-actinide nuclei do not exhibit the resonance pattern characteristic of the giant resonance excitation [2,7]. Although very important for very heavy elements, giant-resonance fission contribution is unimportant for elements with atomic number $Z < 83$ because of the high fission thresholds (22–27 MeV [5]) and small values of the parameter Z^2/A. For nuclei with mass number $A < 210$ the trends of the photofission cross section show, conversely, an increase of several orders of magnitude, for incident energy from the fission threshold ($\sim$20–30 MeV) up to about 200 MeV [7].

Mass-yield distributions for fission of different nuclear systems, which may exhibit symmetric and asymmetric modes and transitions between them, are of particular interest in the investigation of the fission process. It is well known that mass distributions for actinide fission, induced by different projectiles and at intermediate energies, exhibit both symmetric and asymmetric modes. These fission modes can successfully be represented by Gaussian curves, and less than five Gaussian curves were adequate to describe mass distribution of induced fission on pre-actinide and higher actinide nuclei, where increasingly symmetric fission is observed [10]. Although it is well known that fission is predominantly symmetric for pre-actinides with $A \leqslant 227$, since the targets are above the Businaro-Gallone point [11], recently, a new type of asymmetric fission mode was observed in the β-delayed fission of ^{180}Tl using laser ionization with subsequent mass separation [12].

The absence of a reliable theoretical model to predict fission yields, as well as the need for more experimental data, motivated us to investigate photofission processes of pre-actinide nuclei. The essential goal of this paper is to present the measurement of the fragments yields formation from the ^{181}Ta nucleus fission induced by bremsstrahlung photons with endpoint energies of 50 and 3500 MeV. In this experiment the total fission yields for both energies were derived from the experimental yields of fission fragments measured using the off-line induced-activity method. Investigation of

[*]deppman@if.usp.br
[†]ayvgay@if.usp.br
[‡]valdirg@if.usp.br
[§]cgonzaleslorenzo@gmail.com
[‖]balabekyan@ysu.am
[¶]demekhina@nrmail.jinr.ru

photofission on such nuclei is also of importance for practical applications such as astrophysics, medicine, accelerator technology, and nuclear waste transmutation.

Present experimental results for the fission process of the ^{181}Ta nucleus were compared with calculations by the CRISP code based on the multimodal fission approach [13]. This comparison allowed us to extract information on the reaction mechanism related to fission and spallation processes.

II. EXPERIMENTAL PROCEDURE

The data for the photofission cross sections of ^{181}Ta were obtained using bremsstrahlung. The bremsstrahlung with endpoint energies of 3500 and 50 MeV were obtained by using electrons of the Yerevan electron synchrotron and a linear accelerator of the injector type, respectively. The electrons were converted into bremsstrahlung by means of a tungsten converter of about 300 μm (about 0.1 radiation-length units) in thickness. The reaction chamber at the injector was arranged immediately after the converter. The beam-cleaning and beam-formation system consisted of a set of collimators and was used in the irradiation with the high-energy photon beam. The high-energy photon beam passed through the first collimator, 3×3 mm^2 in dimension, and a cleaning magnet, which removed the charged component. The second collimator, 10×10 mm^2 in dimension, was responsible for removing the beam halo. The photon-beam intensity was measured by a Wilson-type quantometer, giving an average of $\sim 10^{11}$ equivalent quanta per second (eq.q s^{-1}) at 3500 MeV and $\sim 10^9$ eq.q s^{-1} at 50 MeV. The photon beam intensities were evaluated from the monitor reactions ^{27}Al$(\gamma, 2pn)^{24}$Na and ^{65}Cu$(\gamma, n)^{64}$Cu, with known cross sections [14,15]. A 0.164-g ^{181}Ta target, with natural isotopic composition (99.98799%) and 0.0487 mm in thickness, was irradiated for 196 and 43 min with the photon beam with endpoint energies 3500 and 50 MeV, respectively.

The yields of radioactive fragments were measured in an off-line analysis using a high-purity germanium (HpGe) detector (80 cm^3) with a resolution of about 0.2% at the ^{60}Co γ-transition energy of 1332 keV. The γ-spectrometer detection efficiencies for four different target-detector distances, namely 0.0, 22.0, 7.0, and 25.0 cm, were determined by using the standard radiation sources of ^{22}Na, ^{54}Mn, ^{57,60}Co, and ^{137}Cs. To obtain the energy dependence of the detector efficiency for energies above 1500 keV, we used also the data from the ^{27}Al$(\gamma, 2pn)^{24}$Na reaction ($E_\gamma = 2754$ keV). The final energy dependence of the HpGe-detector efficiency was obtained with a precision of 10%. Measurements of the γ spectra started about 120 min after the completion of the irradiation and lasted a year. The identification of the reaction products and the determination of their production yield were performed considering the half-lives, energies, and intensities of the γ transitions of the radioactive fragments.

The fragment production yields are considered direct and independent (I) in the absence of a parent isotope contribution (which may give a contribution via $\beta^\pm$ decay) and are determined by the following equation:

$$Y = \frac{\Delta N\ \lambda}{N_p\ N_n\ k\ \epsilon\ \eta\ (1-\exp(-\lambda t_1))\exp(-\lambda t_2)(1-\exp(-\lambda t_3))}, \tag{1}$$

where Y denotes the yields of the reaction fragment production; ΔN is the yield under the photopeak; N_p is the projectile beam intensity (s^{-1}); N_n is the number of target nuclei (in 1/cm^2 units); t_1 is the irradiation time; t_2 is the time between the end of the irradiation and the beginning of the measurement; t_3 is the measurement time; λ is the decay constant (s^{-1}); η is the intensity of γ transitions; k is the total coefficient of γ-ray absorption in target and detector materials; and ϵ is the γ-ray detection efficiency.

If the yield of a given isotope receives a contribution from the $\beta^\pm$ decay of neighboring unstable isobars, the cross section or yield calculation becomes more complicated [16]. If the formation probability for the parent isotope is known from experimental data or if it can be estimated on the basis of other sources, then the independent yields of daughter nuclei can be calculated by the relation

$$\begin{aligned} Y_B = {} & \frac{\lambda_B}{(1-\exp(-\lambda_B t_1))\exp(-\lambda_B t_2)(1-\exp(-\lambda_B t_3))} \\ & \times \left[\frac{\Delta N}{N_\gamma\ N_n\ k\ \epsilon\ \eta} - Y_A\ f_{AB}\ \frac{\lambda_A\ \lambda_B}{\lambda_B - \lambda_A}\left(\frac{(1-\exp(-\lambda_A t_1))\exp(-\lambda_A t_2)(1-\exp(-\lambda_A t_3))}{\lambda_A^2}\right.\right. \\ & \left.\left. - \frac{(1-\exp(-\lambda_B t_1))\exp(-\lambda_B t_2)(1-\exp(-\lambda_B t_3))}{\lambda_B^2}\right)\right], \end{aligned} \tag{2}$$

where the labels A and B refer to the parent and the daughter nuclei, respectively; the coefficient f_{AB} specifies the fraction of A nuclei decaying to a B nucleus (this coefficient gives the information of how much the β decay affects our data; and $f_{AB} = 1$ is when the contribution from the β-decay corresponds to 100%); and ΔN is the total photo peak yield associated with the decays of the daughter and parent isotopes. The effect of the forerunner can be negligible in some limit cases, for example, in the cases where the half-life of the parent nucleus is very long or where the fraction of its contribution is very small. In the case where parent and daughter isotopes could not be separated experimentally, the calculated yields are classified as cumulative (C).

The yield of fission fragment production of ^{181}Ta induced by photon beams with bremsstrahlung energy $E_{\gamma-\max} = 50$ and 3500 MeV are presented in Table I. In total, for the two

TABLE I. Yields of fission fragments measured for the reaction with photons at $E_{\gamma-\max} = 50$ MeV and 3500 MeV on ^{181}Ta target.

Element	Type	Yield, μb/eq.q	
		$E_{\gamma-\max}$=50 MeV	$E_{\gamma-\max}$=3500 MeV
^{59}Fe	C		$\leqslant$10.0
^{64}Cu	I		120 $\pm$ 2.0
^{65}Zn	C		180 $\pm$ 5.0
^{69m}Zn	I		210 $\pm$ 3.0
^{71m}Zn	C		220 $\pm$ 2.0
^{72}Zn	C	013 $\pm$ 0.02	230 $\pm$ 3.0
^{72}Ga	I		$\leqslant$7.2
^{73}Ga	C	014 $\pm$ 0.02	250 $\pm$ 3.7
^{74}As	I	020 $\pm$ 0.03	200 $\pm$ 4.0
^{75}Se	C		290 $\pm$ 4.0
^{76}As	I	020 $\pm$ 0.03	220 $\pm$ 3.0
^{77}Ge	C	020 $\pm$ 0.03	290 $\pm$ 4.0
^{77}Br	I		$\leqslant$5.0
^{78}Ge	C	025 $\pm$ 0.04	220 $\pm$ 2.2
^{78}As	I		150 $\pm$ 2.3
^{82}Br	I		230 $\pm$ 4.0
^{84}Br	C	040 $\pm$ 0.06	310 $\pm$ 6.0
^{84}Rb	I		40 $\pm$ 0.7
^{84m}Rb	I		$\leqslant$5.0
^{85m}Sr	C		270 $\pm$ 5.0
^{86}Rb	I	036 $\pm$ 0.05	150 $\pm$ 3.0
^{87}Kr	C	045 $\pm$ 0.07	330 $\pm$ 3.3
^{87}Y	C		$\leqslant$8.8
^{88}Kr	C	040 $\pm$ 0.06	300 $\pm$ 6.0
^{88}Y	I		$\leqslant$7.0
^{88}Zr	C		$\leqslant$10.0
^{90m}Y	C		410 $\pm$ 6.0
^{91}Sr	C	038 $\pm$ 0.06	350 $\pm$ 7.0
^{91m}Y	C		$\leqslant$9.0
^{92}Sr	C	036 $\pm$ 0.05	330 $\pm$ 7.0
^{92}Y	I		$\leqslant$7.0
^{93}Y	C	029 $\pm$ 0.04	360 $\pm$ 6.0
^{95}Zr	C	040 $\pm$ 0.06	340 $\pm$ 5.0
^{95m}Nb	I		90 $\pm$ 1.4
^{96}Nb	I		320 $\pm$ 5.0
^{96}Tc	I		$\leqslant$4.0
^{97}Zr	C	028 $\pm$ 0.04	270 $\pm$ 5.4
^{99}Mo	C	027 $\pm$ 0.04	290 $\pm$ 6.0
^{100}Pd	C		130 $\pm$ 2.6
^{102}Rh	C		220 $\pm$ 5.0
^{103}Ru	C	015 $\pm$ 0.03	250 $\pm$ 5.0
^{105}Ru	C	015 $\pm$ 0.03	130 $\pm$ 2.6
^{105}Rh	I		$\leqslant$4.0

energies measured, 61 yields were calculated for the fragment mass region $70 < A < 100$ u. The quoted uncertainties in the experimental yields are from the contributions of the statistical uncertainty ($\leqslant$2–3%), uncertainty in the target thickness ($\leqslant$3%), and uncertainty in the detector efficiency ($\leqslant$10%).

III. RESULTS AND DISCUSSION

From the production yields of the individual fragments we can construct the mass-yield distribution (yield of each isobar as a function of the mass number A). However, to obtain the yield for each isobar with mass A, it is necessary to estimate the yield of the isotopes not measured by the induced-activity method. The yields for these fragments can be obtained from the analysis of the charge distribution of the corresponding isobar chain, i.e., the yields as a function of Z for a given A. We assumed that the charge distribution can be well described by a Gaussian function characterized by the most probable charge, Z_P (centroid of the Gaussian function), of an isobaric chain with mass A and the associate width, Γ_Z. Moreover, the assumption is made that the most probable charge as well as the width of the charge distribution vary linearly with the mass of the fission fragment. The following parametrization of the production yield as a function of the charge of the fission fragment is adopted [10]:

$$Y_{A,Z} = \frac{Y_A}{\Gamma_Z \pi^{1/2}} \exp\left(-\frac{(Z - Z_P)^2}{\Gamma_Z^2}\right), \tag{3}$$

where $Y_{A,Z}$ is the independent yield of the nuclide (Z, A). The values Y_A stands for the total isobaric yield for given mass number A, Z_P is the most probable charge for the charge distribution of an isobars with mass number A, and Γ_Z is the corresponding width parameter. The values Z_P and Γ_Z can be represented as slowly varying linear functions of the mass numbers of fission fragments:

$$Z_P = \mu_1 + \mu_2 A, \tag{4}$$

$$\Gamma_Z = \gamma_1 + \gamma_2 A, \tag{5}$$

where μ_1, μ_2, γ_1, and γ_2 are adjustable parameters determined by considering a systematic analysis of the fission fragments. The obtained values for these parameters are listed in Table II.

TABLE II. Parameter values obtained for the mass and charge distributions for the ^{181}Ta target at the endpoint energies of 50 and 3500 MeV.

Parameter	50 MeV	3500 MeV
$(\lambda_A)_{\text{exp}}$	000040 $\pm$ 0.00001	00410 $\pm$ 0.0002
$(\lambda_A)_{\text{cal}}$	0.0004	
$(M_A)_{\text{exp}}$	880 $\pm$ 0.6	850 $\pm$ 0.6
$(M_A)_{\text{cal}}$	87.9	82.5
$(\Gamma_A)_{\text{exp}}$	1439 $\pm$ 0.20	235 $\pm$ 0.3
$(\Gamma_A)_{\text{cal}}$	15.0	
$(\mu_1)_{\text{exp}}$	1.69 $\pm$0.11	0779 $\pm$ 0.046
$(\mu_1)_{\text{cal}}$	1.690	
$(\mu_2)_{\text{exp}}$	0397 $\pm$ 0.002	0420 $\pm$ 0.001
$(\mu_2)_{\text{cal}}$	0.397	
$(\gamma_1)_{\text{exp}}$	0590 $\pm$ 0.007	0590 $\pm$ 0.003
$(\gamma_1)_{\text{cal}}$	0.59	
$(\gamma_2)_{\text{exp}}$	00050 $\pm$ 0.0009	00050 $\pm$ 0.0004
$(\gamma_2)_{\text{cal}}$	0.0050	

The mass-yield distribution (isobaric yields) of fission fragments were then constructed by using the obtained values of Y_A for each isobar chain. These mass distribution for the two endpoint energies are plotted in Figs. 1 and 2, respectively. In these figures the experimental data points of the present work are

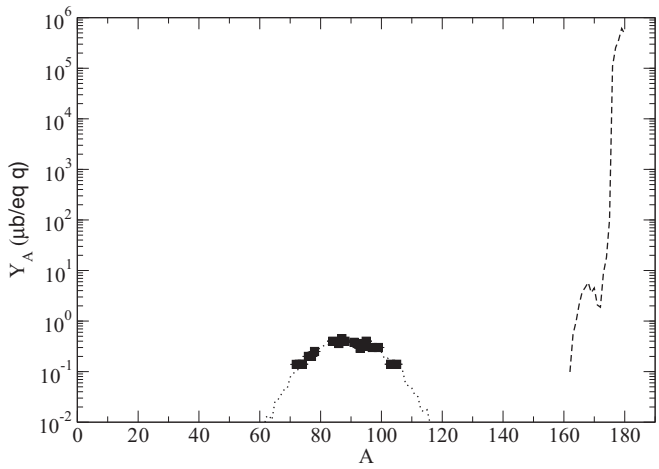

FIG. 1. Mass-yield distribution for photofission of ^{181}Ta at endpoint energy of 50 MeV. The present experimental data are shown by solid square symbols and the results of CRISP code calculation for fission and spallation are given by the dotted line curve and the dashed line curve, respectively.

represented by black square symbols. In Fig. 2 we also present the data from Ref. [17], including data from spallation process of Ta target fragmentation (^{9}Be, ^{22,24}Na, and $A > 120$ u) at bremsstrahlung endpoint energy of 4 GeV (open circles).

As one can see in both Figs. 1 and 2, data in the expected mass region for fission fragments agree with the assumption of a symmetric mass distribution. This mass region was then fitted with a Gaussian shape function given by

$$Y_f = \lambda_A \exp\left(-\frac{(A - M_A)^2}{\Gamma_A^2}\right) \tag{6}$$

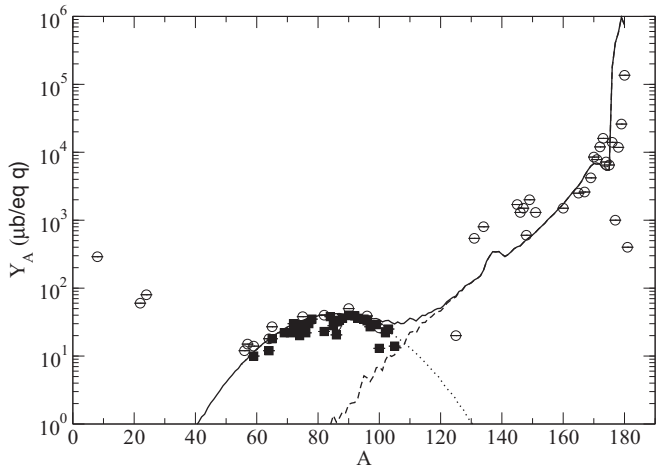

FIG. 2. Mass-yield distribution of photofission of ^{181}Ta at endpoint energy of 3500 MeV. The present experimental data are shown by the solid square symbols. The open circle symbols correspond to data taken from Ref. [17], which also include spallation contributions. The results of the CRISP code calculation for fission and spallation are given by the dotted line and the dashed line curve, respectively. The black solid line indicates the sum of the calculated fission and spallation yields.

where the parameter λ_A is the height, M_A is the average mass number, and Γ_A is the width of the Gaussian. These parameters were adjusted to the data and the obtained values are listed in the Table II as $(M_A)_{\text{exp}}$ and $(\Gamma_A)_{\text{exp}}$ for each endpoint energy. The width as well as the height of the mass distribution clearly increase with increasing photon energy. From the mean value of the mass distributions, we can also conclude that, on average, three mass units are emitted from both fissioning nuclei and fission fragments at the energy of 50 MeV and six mass units are emitted for the photon endpoint energy of 3500 MeV.

The integration over the Gaussian gives the experimental fission yields for each endpoint energy. Actually, to get the fission yields, we had to multiply the Gaussian integration by a factor of 0.5 to take into account the double counting in the yields due to the two fission fragments in each event. The experimentally determined values for fission yield for the endpoints energies 50 and 3500 MeV are, in units of μbarn and mbarn per equivalent quanta, $Y_f = 5.4 \pm 1.1$ μb/eq.q and $Y_f = 0.77 \pm 0.11$ mb/eq.q, respectively. The fission yield of the present work at energy of 3500 MeV agrees well with the value of 0.64 ± 0.06 mb/eq.q obtained for reaction of bremsstrahlung with endpoint energy of 3770 MeV on ^{181}Ta [18].

From our data we could also estimate the fissility defined as the ratio of total fission yield to total nuclear photoabsoption yield ($D = Y_f/Y_{\text{abs}}$). To determine Y_{abs} it is necessary to take into account all possible decay channels of the excited nucleus being considered. The calculated fissility from our experimental fission yield for the 50-MeV endpoint photons is $(0.23 \pm 0.05) \times 10^{-3}$ and for 3500 MeV is $(2.9 \pm 0.5) \times 10^{-3}$. Here we considered the photoabsorption yield for the endpoint energy 3500 MeV by taking the average value of data above the quasideuteron region of photonuclear absorption from Refs. [3,4,8]. The fissility obtained for bremsstrahlung endpoint energy of 50 MeV is consistent with the trends calculated for photofission on $^{\text{nat}}$Ta induced by monochromatic photons of 69 MeV [5] and for photofission of ^{181}Ta at an incident monochromatic photon energy of 100 MeV [7]. The fissility for the higher endpoint energy (3500 MeV) is in agreement with the systematics of fissilities as a function of Z^2/A for photofission reactions with Ta targets at intermediate energies up to 6.0 GeV [3]. A general trend of increasing fissility with increasing photon energy for pre-actinide nuclei is consistent with what the results of a systematic investigation of fission induced by bremsstrahlung on Bi, Pb, Ti, Au, Pt, Os, Re, Ta, and Hf target nuclei [19].

IV. CALCULATION WITH CRISP CODE

Calculations of fission cross sections and yields within different models have provided good opportunities to estimate the validity of the various reaction mechanisms and to investigate characteristics of the processes taking place in reactions induced by different probes. Here we used the simulation code CRISP [20] to analyze our data. CRISP is a Monte Carlo model code to describe nuclear reactions that uses a two-step process [21,22]. First, an intranuclear cascade is simulated, following a time-ordered sequence of collisions

in a many-body system [13,23,24]. When the intranuclear cascade finishes, the nucleus thermalizes and the competition between evaporation (of nucleons and α particles) and fission starts. This code was recently used to analyze fission reactions induced by protons and photons [25–27].

The fission fragment distribution is calculated according to the random neck rupture model [28], where the combination of a liquid-drop model with the nuclear shell structure produces valleys in the phase space of the deforming nucleus and where the fission dynamics can develop, leading to different fragments after the scission point. The fragment mass distributions for the different channels are described in the model as a Gaussian characterized by peak position and width that are used as free parameters to fit experimental data. In Refs. [25–27] this model is used to fit the experimental data on fission fragment distribution. After the fission fragments are formed, their excitation energies are calculated and the evaporation process allows for de-excitation through what we call postscission evaporation [25–27]. The evaporation from fragments follow the same theoretical approach as for the compound nucleus formed at the beginning of the reaction.

To analyze the present data we pushed the code to simulate not only the fission process but also the spallation reaction, which might be an important reaction channel for proton- and photon-induced reactions at intermediate energies. The results of the CRISP calculations for both fission and spallation processes for our data on ^{181}Ta target, at two endpoint energies, are shown in Figs. 1 and 2. The results of the simulation for fission calculation, given by the dotted line, show clearly that the experimental distributions for both endpoint energies, taking into account only the intermediate mass (fission fragment) region, can be well reproduced by a single symmetric Gaussian curve. Both peak position and width of the distributions are well described by the CRISP model. We used for the fission calculation the experimental parameters of the charge distribution listed in Table II. For the mass distribution at endpoint energy of 50 MeV, the small fluctuations in the calculation is due to a limitation in the statistics. Although 5×10^6 events were simulated, the resulting statistics for the fission of ^{181}Ta is low due to the small fission yields.

The total fission yields for ^{181}Ta, as calculated by CRISP, are 5.3 μb/eq.q and 0.81 mb/eq.q at low and intermediate energies, respectively, which agree with our experimental values obtained by a Gaussian fitting procedure described in the previous section. As can be observed in Table II, the mean value for the mass distribution in the 3500-MeV case is shifted to about two mass units below the experimental value, while in the case of 50 MeV there is a good agreement between the corresponding calculated and experimental values. These results indicate that the CRISP model is underestimating the yield of the heavier fission fragments at the high-energy region, since the main difference between the two endpoint energies is the existence of more high-energy photons for 3500 MeV than for 50 MeV. In order to trace back the possible origin of this discrepancy in our calculation we have to consider that a reduced fragment yield in the heavier mass sector can have two main causes: an overestimation of prescission evaporation or an overestimation of postscission evaporation. The comparison between calculated and experimental neutron multiplicity is performed below and allows us to understand the possible origin of the problem in the mean mass of fission fragments for the 3500-MeV case.

The results of the CRISP calculation for the spallation process are indicated by dashed lines in the Figs. 1 and 2. The black solid line in Fig. 2 indicates the sum of the calculated fission and spallation yields. As can be observed in Fig. 2, CRISP model does not give satisfactory results for the very light mass fragment region, and since nuclear fragmentation is not included in the model, this may be an indication that the fragmentation is relevant for explaining the fragment production in the mass range of 1–20 mass units.

CRISP calculations enables us to extract the fissility for 50- and 3500-MeV endpoint bremsstrahlung energies, which are 0.16×10^{-3} and 0.41×10^{-3}, respectively. A qualitative agreement is obtained between the experimental and calculated fissility value for the low-energy photofisison. For the high-energy photofission, the experimental fissility value is about one order of magnitude higher than the calculated value. A possible explanation for this is the fact that the total photon absorption yield is being overestimated by CRISP code due to a limitation of the model in taking into account all possible channels of decay of the excited target nucleus being considered.

Another source of information about the reaction dynamics that can be obtained from the simulation is the neutron production. The emission of neutrons starts already at the intranuclear cascade process with the pre-equilibrium production followed by the evaporation of neutrons from an equilibrated composite system. Both categories are referred to as prescission neutrons [29]. The postscission neutrons are obtained when the system passes the scission point with neutron emission by the residual fragments. The neutron production can then have the following contributions:

(i) from the composite system;
(ii) during the transition of the composite system through the saddle-point configuration towards the scission point;
(iii) during the neck rupture;
(iv) from the accelerating fragments; and
(v) after completion of their acceleration.

The contributions from (i), (ii), and (iii) are not distinguishable and are therefore considered as prescission neutrons. The contributions from (iv) and (v) are classified as postscission neutrons. With the CRISP model we can also obtain the average number of pre- and postscission emitted neutrons. We present in Table III the average fissioning nucleus mass A_f, the average mass after evaporation A_{ff}, as well as the average numbers of pre- and postscission neutrons. The sum of the two neutron emission contributions gives the total number of emitted neutrons, which can be compared with the experimental values in Table III. We observe a good agreement between the calculated and the experimental values for the low-energy-induced fission, showing that the theoretical predictions for the emission of neutrons are correct. However, for the higher energy (3500 MeV) the calculation of the neutron multiplicities from the excited

TABLE III. Calculated and experimental parameters obtained for the mass distribution: mean mass of the fissioning nucleus $[(A_f)_{cal}]$ after evaporation of prescission neutrons from the compound nucleus; mean mass of the fissioning nucleus $[(A_{ff})_{cal}]$ after evaporation of postscission neutrons from fragments; experimental mean mass of the fissioning nucleus $[(A_{ff})_{exp}]$, which includes both types of evaporated neutrons; numbers of pre- and post-scission neutrons; number evaporated from the excited nucleus; and total fission yields.

Parameter	50 MeV	3500 MeV
$(A_{ff})_{exp}$	176.0 ± 0.9	1700 ± 0.9
$(A_{ff})_{cal}$	175.8	165.0
$(A_f)_{cal}$	180.4	178.3
(Prescission neutrons)$_{cal}$	0.6	2.7
(Postscission neutrons)$_{cal}$	4.6	13.3
(Evaporated neutrons)$_{exp}$	5.0 ± 4.0	11.0 ± 1.2
(Fission yield)$_{exp}$	5.4 ± 1.1 μb/eq.q	0.77 ± 0.11 mb/eq.q
(Fission yield)$_{cal}$	5.3 μb/eq.q	0.81 mb/eq.q

^{181}Ta nucleus is somewhat overestimated. The experimental neutron emission is 11 neutrons while the calculation gives 16 neutrons. Again we emphasize that as the intranuclear cascade and the evaporation/fission chains are larger, the calculation is more difficult. In this case, however, it is possible to observe that the main contribution to the disagreement between calculation and experiment comes from the fission fragment evaporation (postscission neutrons). There are some points in the calculation which could lead to this discrepancy, but most of them are also present in the evaporation of the compound nucleus formed after the intranuclear cascade. There is one particular mechanism which is related only to the fragment evaporation, namely, the distribution of the excitation energy between the two fission fragments. In the CRISP model it is assumed that the excitation energy of the fissioning nucleus will be distributed to the two fragments proportionally to their masses, keeping the total excitation energy constant. Behind this assumption is the idea that there is no energy transfer in the scission process from microscopic to collective degrees of freedom. This is not necessarily true, and the large number of neutrons evaporated from the fragments may be an indication that part of the excitation energy may appears as collective motion of the fragments. We are working on this issue to improve the simulation code CRISP, but we can say that the present analysis with the CRISP code already indicates that our theoretical model gives a good description of the dynamical process taking place inside the nucleus during reactions at intermediate energies.

V. CONCLUSION

In this work we present the results of the investigation of the induced fission of ^{181}Ta nucleus by bremsstrahlung with endpoint energies of 50 and 3500 MeV. Photofission yields have been measured by taking advantage of the induced-activity method in an off-line analysis. The total photofission yields have been determined for the two very different energy regimes, taking into account the measured photon spectrum. Photofissility values were subsequently deduced for each endpoint energy of photons. The obtained total fission yields and fissility values have been found to agree quite well with the values obtained from measurements at 69 and 3770 MeV of incident photon energies. An analysis of the charge and mass distribution of fission fragments from the ^{181}Ta target have been performed with the CRISP code. The comparison between calculated parameters for the ^{181}Ta target and the experimental data has shown that the CRISP model gives a good description of the main characteristics of the reaction under investigation at the both endpoint energies (50 and 3500 MeV). A small disagreement between experimental and calculated values was found for the neutron evaporation from the hot fission fragments. We argue that this problem can be related to the transfer of energy from microscopic to collective degrees of freedom in the fissioning system, which is being improved in the CRISP code.

ACKNOWLEDGMENTS

G. Karapetyan is grateful to Fundação de Amparo à Pesquisa do Estado de São Paulo (FAPESP 2011/00314-0 and 2014/00284-1) and also to International Centre for Theoretical Physics (ICTP) under the associate grant scheme. A. Deepman and V. Guimaraes acknowledge support from CNPq under Grants No. 305639/2010-2 and No. 302969/2013-6, respectively.

[1] T. Methasiri and S. A. E. Johansson, Nucl. Phys. A **167**, 97 (1971).
[2] I. Kroon and B. Forkman, Nucl. Phys. A **197**, 81 (1972).
[3] D. A. De Lima, J. B. Martins, and O. A. P. Tavares, Nuovo Cimento A **103**, 701 (1990).
[4] V. Emma, S. Lo Nigro, and C. Milone, Nucl. Phys. A **257**, 438 (1976).
[5] O. A. P. Tavares, J. B. Martins, E. de Paiva *et al.*, J. Phys. G: Nucl. Part. Phys. **19**, 805 (1993).
[6] J. B. Martins, E. L. Moreira, O. A. P. Tavares *et al.*, Nuovo Cimento A **101**, 789 (1989).
[7] M. L. Terranova, O. A. P. Tavares, G. Ya. Kezerashvili *et al.*, J. Phys. G: Nucl. Part. Phys. **22**, 511 (1996).
[8] M. L. Terranova, G. Ya. Kezerashvili, A. M. Milov *et al.*, J. Phys. G: Nucl. Part. Phys. **24**, 205 (1998).
[9] E. de Paiva, O. A. P. Tavares, and M. L. Terranova, J. Phys. G: Nucl. Part. Phys. **27**, 1435 (2001).
[10] M. C. Duijvestijn, A. J. Koning, J. P. M. Beijers, A. Ferrari, M. Gastal, J. van Klinken, and R. W. Ostendorf, Phys. Rev. C **59**, 776 (1999).
[11] U. L. Businaro and S. Gallone, Nuovo Cimento **1**, 629 (1955).

[12] A. N. Andreyev *et al.*, Phys. Rev. Lett. **105**, 252502 (2010).
[13] A. Deppman, S. B. Duarte, G. Silva *et al.*, J. Phys. G **30**, 1991 (2004).
[14] K. Masumoto, T. Kato, and N. Suzuki, Nucl. Instrum. Methods Phys. Res. **157**, 567 (1978).
[15] A. S. Danagulyan and N. A. Demekhina, Yad. Fiz. **24**, 681 (1976) [Sov. J. Nucl. Phys. **24**, 355 (1976)].
[16] H. Baba, J. Sanada, H. Araki *et al.*, Nucl. Instrum. Methods A **416**, 301 (1998).
[17] K. A. Amroyan, S. A. Barsegyan, and N. A. Demekhina, Yad. Fiz. **56**, 4 (1993) [Phys. Atomic Nuclei **56**, 1 (1993)].
[18] G. A. Vartapetyan, N. A. Demekhina, V. I. Kasilov *et al.*, Sov. J. Nucl. Phys. **14**, 37 (1972).
[19] Yu. N. Ranyuk and P. V. Sorokin, Yad. Fiz. **5**, 37 (1967) [Sov. J. Phys. **5**, 26 (1967)].
[20] A. Deppman, O. A. P. Tavares, S. B. Duarte *et al.*, Comp. Phys. Commun. **145**, 385 (2002).
[21] A. Deppman, O. A. P. Tavares, S. B. Duarte, J. D. T. Arruda-Neto, M. Gonçalves, V. P. Likhachev, and E. C. de Oliveira, Phys. Rev. C **66**, 067601 (2002).
[22] A. Deppman, O. A. P. Tavares, S. B. Duarte *et al.*, Nucl. Instr. Meth. B **211**, 15 (2003).
[23] T. Kodama, S. B. Duarte, K. C. Chung, and R. A. M. S. Nazareth, Phys. Rev. Lett. **49**, 536 (1982).
[24] M. Goncalves, S. de Pina, D. A. Lima *et al.*, Phys. Lett. B **406**, 1 (1997).
[25] A. Deppman, E. Andrade II, V. Guimarães, G. S. Karapetyan, A. R. Balabekyan, and N. A. Demekhina, Phys. Rev. C **88**, 024608 (2013).
[26] A. Deppman, E. Andrade II, V. Guimarães, G. S. Karapetyan, and N. A. Demekhina, Phys. Rev. C **87**, 054604 (2013).
[27] A. Deppman *et al.*, Phys. Rev. C **88**, 064609 (2013).
[28] U. Brosa, S. Grossman, and A. Muller, Z. Naturforsch. A **41**, 1341 (1986).
[29] M. Strecker, R. Wien, P. Plischke, and W. Scobel, Phys. Rev. C **41**, 2172 (1990).